Electronic Relaxation Pathways in Heavy-Atom-Free Photosensitizers Absorbing Near-Infrared Radiation and Exhibiting High Yields of Singlet Oxygen Generation

Luis A. Ortiz-Rodríguez,[1] Sean J. Hoehn,[1] Axel Loredo,[2] Lushun Wang,[2] Han Xiao,[2,3,4] Carlos E. Crespo-Hernández*,[1]

[1] Department of Chemistry, Case Western Reserve University, Cleveland, Ohio, 44106, USA
[2] Department of Chemistry, Rice University, Houston, Texas, 77005, USA
[3] Department of Biosciences, Rice University, Houston, Texas, 77005, USA
[4] Department of Bioengineering, Rice University, Houston, Texas, 77005, USA

* email of corresponding author: carlos.crespo@case.edu

Abstract

Heavy-atom-free photosensitizers based on thionation of carbonyl groups of readily accessible organic compounds are rapidly emerging as a versatile class of molecules. However, their photochemical properties and electronic relaxation mechanisms are currently poorly understood. Investigating the excited-state dynamics and electronic relaxation mechanisms is essential to fully understand their benefits and limitations, and to refine the photochemical properties therein of to be developed photosensitizers. In this Communication, the photochemical and electronic-structure properties of thio-4-dimethylaminonaphthalamide and thionated Nile Red, two of the most promising heavy-atom-free photosensitizers developed to date, are revealed. Steady-state and time-resolved transient absorption techniques are combined with ground and excited state calculations of electronic excited states that are populated upon near-infrared excitation to elucidate their photochemistry. It is shown that excitation of these photosensitizers with near-infrared radiation leads to the efficient population of the triplet manifold through multiple relaxation pathways in hundreds of femtoseconds. The remarkably strong coupling between the singlet and triplet states in both the Franck-Condon and local minima regions of their excited state potential energy surfaces are anticipated to enable a broad-range of applications for this new family of photosensitizers, including in photodynamic therapy, photocatalysis, photovoltaics, organic LEDs, and photon up-conversion.

Photodynamic therapy (PDT) is a clinically approved, noninvasive therapeutic modality for the treatment of cancers that relies on the administration of a photoactivable drug (a.k.a., photosensitizer, PS) and light to the affected area.[1-5] Light absorption by the PS promotes intersystem crossing (ISC) to its triplet state, which can transfer its energy to molecular oxygen, generating singlet oxygen and other reactive oxygen species (ROS) that are toxic to the targeted cancer cells and tissues. PDT is more attractive than conventional therapies such as surgery, radiotherapy, and chemotherapy, because of its minimally invasive nature, exceptional spatiotemporal selectivity, diminished side effects, feasibility of repeated treatments with superior cosmetic outcomes, and overall simplicity of the technique among other important considerations.[4, 6-8] Notwithstanding these significant benefits over traditional therapies, PDT has yet to reach its full potential primarily because optimal photosensitizers, applicable to a wide range of cancers and biological tissues, are difficult to develop. Among other requirements, an ideal PS should be easy to synthesize and storage,[9] has a high molar absorptivity in the therapeutic window (ca. 600 to 800 nm),[10] a high triplet yield and low cytotoxicity in the dark, produce a high singlet oxygen quantum yield, and be cost effective.[5, 9, 11]

One prevalent approach to develop prospective PSs is to incorporate heavy atoms into biocompatible organic molecules to enhance their ISC efficiency. These compounds, however, are often difficult to synthesize, costly, and suffer from increased dark cytotoxicity.[12-14] Another approach that is swiftly gaining increased attention is to substitute the oxygen atom of carbonyl groups with sulfur of existing organic molecules to red-shift and increase their molar absorptivity coefficients, enhance triplet state population, and the production of singlet oxygen and ROS.[5, 15-18] Many of these new generation of thionated or heavy-atom-free PSs (HAF-PSs), have been demonstrated to offer good biocompatibility, biodegradability, minimum dark cytotoxicity, and structural stability.[5, 16, 18-20] Two highly promising HAF-PSs that have been developed recently (Figure 1), are thio-4-dimethylaminonaphthalamide (SDMNP) and thionated Nile Red (SNR).[18, 21] These HAF-PSs have been demonstrated to exhibit high absorption cross-sections in the near infrared (NIR), high yield of singlet oxygen generation, and good PDT efficacy against monolayer cancer (HeLa) cells and 3D multicellular tumor spheroids.[18] However, the photochemical properties that make these molecules highly promising HAF-PSs are currently unknown, particularly, their electronic relaxation mechanisms upon NIR-excitation. Elucidating the excited-state dynamics and relaxation mechanisms of these HAF-PSs is essential for diagnosing their benefits and limitations, and to further refine this chemistry.

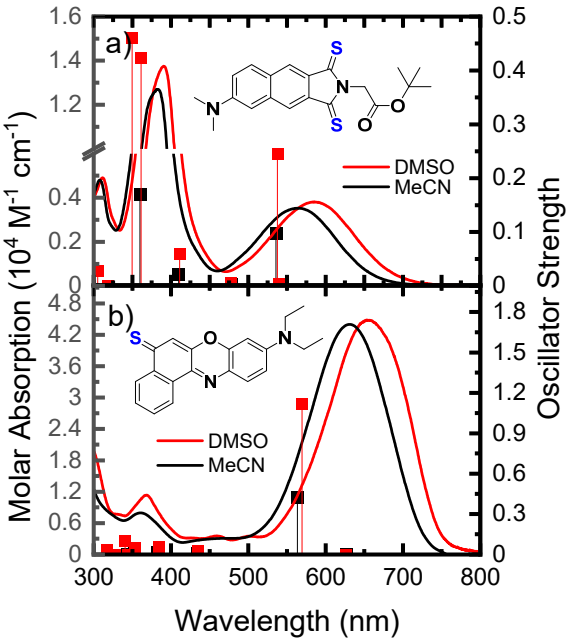

Figure 1. Ground-state absorption spectra of a) SDMNP and b) SNR in dimethylsulfoxide (DMSO) and acetonitrile (MeCN) normalized to their lowest-energy $\pi \rightarrow \pi^*$ transitions. Vertical lines correspond to the calculated absorption spectra (i.e., electronic transitions and corresponding oscillator strengths) of both compounds at the TD-PBE0/IEFPCM/6-31+G(d,p)//B3LYP/IEFPCM/6-31+G(d,p) in each solvent. Inset: molecular structure of SDMNP and SNR.

Figure 1 shows the molecular structures and absorptivity spectra of SDMNP and SNR in dimethylsulfoxide (DMSO) and acetonitrile (MeCN). Importantly, the absorptivity spectrum of SDMNP extends to 725 and 750 nm in MeCN and DMSO, respectively, while it extends to 750 and 795 nm for SNR. Both molecules exhibit negligible fluorescence quantum yields (< 0.001) and generate high singlet oxygen quantum yields–81% and 36% for SDMNP and SNR, respectively.[18, 21]

An important step in the development of prospective HAF-PSs is to characterize their photophysical properties and the electronic pathways that are available for ISC to the reactive triplet state. With this aim in mind, vertical excitation energies (VEEs) were calculated for SDMNP and SNR to characterize the electronic transitions that are accessible following excitation with NIR. The calculated VEEs are shown in Figure 1 and in Tables S1 and S2 for SDMNP and SNR, respectively. Excitation of these HAF-PSs with NIR populates the lowest energy $\pi\pi^*$ electronic state (S_2) in both solvents, while the S_1 state has $n\pi^*$ character and negligible oscillator strength in both molecules. The VEEs rationalize the negligible fluorescence quantum yield measured for both molecules.[18]

The calculations also show that there are four and three triplet states lower in energy than the $S_2(\pi\pi^*)$ state in SDMNP and SNR, respectively. Hence, the population reaching the $S_2(\pi\pi^*)$ state can in principle relax from the Franck-Condon (FC) region through at least five electronic states in SDMNP or through four electronic states in SNR. Furthermore, within the expected

accuracy (± 0.3 eV), the calculations predict that $S_2(\pi\pi^*)$ state is isoenergetic with the $S_1(n\pi^*)$ and the $T_4(n\pi^*)$ states in SDMNP, while the $S_1(n\pi^*)$ state is isoenergetic with the $T_3(\pi\pi^*)$ state in SNR. The near degeneracy of these states suggests that they are strongly coupled in the FC region and may give rise to nonradiative relaxations pathways that efficiently populate the triplet manifold in both molecules.

To investigate this possibility further, the spin-orbit coupling constants (SOCs) between the two lowest energy excited singlet states and the four/three triplet states of SDMNP/SNR were calculated from three key regions of their potential energy surfaces (PESs): the FC, the S_1-minimum, and the S_2-minimum (Tables S3 and S4). Based on the magnitude of the SOCs and the El Sayed's propensity rules,[22-23] ISC to the triplet manifold in SDMNP is predicted to occur more efficiently between the S_2 and T_3 states and between the S_1 and T_1 states, independent of the regions of the PESs or solvent used, while ISC between the S_2 and the T_4 states may also play a smaller role. Similarly, ISC to the triplet manifold in SNR is predicted to occur more efficiently between the S_2 and T_2 states, the S_1 and T_1 states, and the S_1 and T_3 states, independent of the regions of the PESs or solvent used. The multitude of ISC pathways predicted to play a major role is remarkable and confirms the increased density of states upon thionation. It also lends support to the idea that these singlet and triplet states are strongly coupled and may give rise to efficient and near unity triplet state yields in both molecules.

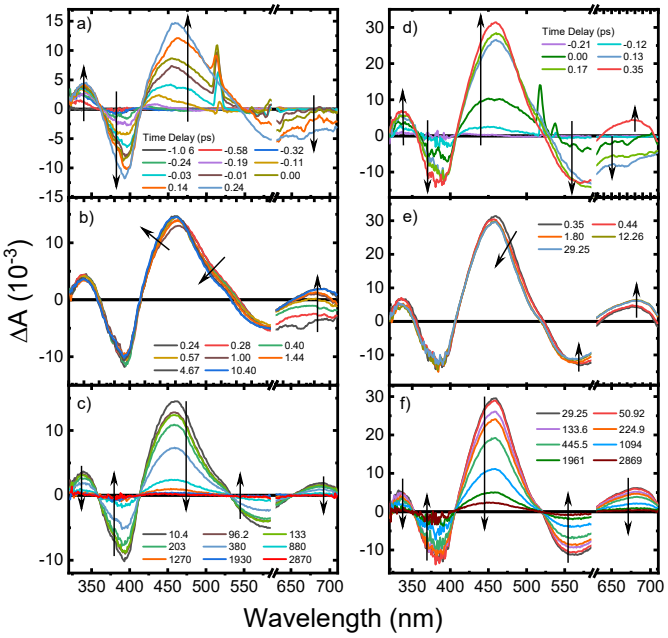

Figure 2. fs-TAS for SDMNP following excitation at 610 nm in (a-c) DMSO and (d-f) MeCN solutions. Stimulated Raman emission bands from the solvent are observed with the cross-correlation of the pump and probe beams around 510 in DMSO and around 520 nm in MeCN, respectively. The breaks are covering the scattering of the pump beam reaching the detectors.

To experimentally investigate if ISC occurs efficiently and independent of solvent, transient absorption spectroscopy (TAS) experiments with femtosecond time resolution were collected. Figure 2 presents the spectral evolution for SDMNP following 610 nm excitation. Two positive and two negative amplitude bands are observed within the cross-correlation of the pump

and probe beams (Figure 2a,d). The negative amplitude bands are assigned to S_0 depopulation, in good agreement with the absorption spectra (Figure 1a). The positive amplitude bands are assigned to excited state absorption (ESA) by transient species. One of the bands exhibits a maximum at ca. 340 nm, while the other has a maximum around 460 nm. In DMSO, both bands reach their maximum intensity around 240 fs, while in MeCN, they reach their maximum intensity around 350 fs. A blueshift of the 460 nm band is observed (Figure 2b,e), while a new absorption band appears simultaneously with a maximum around 680 nm. The positive amplitude absorption bands decay monotonically during the temporal window between ca. 11 ps to 3 ns in DMSO, or ca. 30 ps to 3 ns in MeCN, while S_0 repopulation is simultaneously observed. Representative decay traces, lifetimes extracted from kinetic analyses, and the corresponding evolution associated difference spectra (EADS) are reported in Figure 3(a,b), Table 1, and Figure S1, respectively.

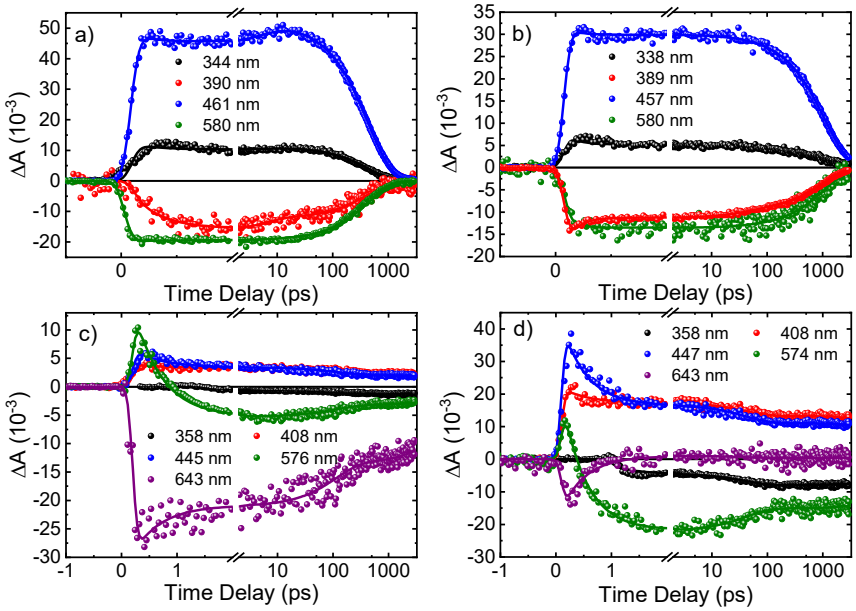

Figure 3. Representative decay traces for SDMNP in (a) DMSO and (b) MeCN and for SNR in (c) DMSO and (d) MeCN. The solid lines are the fittings obtained with the global and target analysis of the multidimensional transient absorption data (see Methods in the SI for details).

Based on the calculations, excitation at 610 nm populates the $S_2(\pi\pi^*)$ state directly, which is isoenergetic to the $S_1(n\pi^*)$ and $T_3(n\pi^*)$ states (Table S1). To assist in the assignment of the transient species, the $S_2(\pi\pi^*)$, $S_1(n\pi^*)$, and $T_1(\pi\pi^*)$ states were optimized and their ESA were calculated (Figure S2). Attempts to optimize the $T_3(n\pi^*)$ state were unsuccessful. The ESA demonstrate that the absorption spectra of both singlet states and the $T_1(\pi\pi^*)$ state overlap significantly, while the ESA from the singlet excited states are largely blue-shifted relative to that of the $T_1(\pi\pi^*)$ state. Hence, we assign the absorption 460 nm band to the vibrationally excited $T_1(\pi\pi^*)$ and/or the $T_3(n\pi^*)$ states, with some overlap with the $S_2(\pi\pi^*)$ and $S_1(n\pi^*)$ states. The 339 nm band has significant overlap from both $S_1(n\pi^*)$ and $S_2(\pi\pi^*)$ states. A comparison of decay traces at 339 and 460 nm support this idea (Figure 3a,b). The band observed between 400 to 525 nm redshifts and grows within the cross-correlation of the pump and probe beams (Figures 2a,d and 3). The redshift is assigned to population of the $S_2(\pi\pi^*)$ state and ultrafast internal conversion

(IC) to the $S_1(n\pi^*)$ state, competing with ISC to the triplet manifold from both singlet states. Indeed, considering the El Sayed's rules, the large SOCs, and the dynamics observed in the TAS, it becomes evident that population of the triplet manifold occurs through two competitive relaxation pathways. One is a direct $S_2(\pi\pi^*) \rightarrow T_3(n\pi^*)$ ISC pathway, with subsequent IC to the $T_1(\pi\pi^*)$ state. The other is an indirect $S_2(\pi\pi^*) \rightarrow S_1(n\pi^*) \rightarrow T_1(\pi\pi^*)$ ISC pathway, where IC occurs initially, followed by ISC to the $T_1(\pi\pi^*)$ state. Remarkably, both pathways are occurring within 580 and 210 fs (τ_1) in DMSO and MeCN, respectively. The ultrafast ISC lifetime lends strong support to the idea that triplet state of SDMNP is populated in high yield, as observed previously for a wide-range of thiobase derivatives[15-16, 24-33] and other thionated compounds.[34-36]

The blueshift observed in Figure 2b,e is assigned to a combination of vibrational cooling (VC) and solvent relaxation (SR) dynamics in the triplet manifold. The large $\Delta E(S_1\text{-}T_1)$ and $\Delta E(T_3\text{-}T_1)$ energy gaps (Table S1) and the observation that τ_2 changes significantly with solvent (Table 1), support this assignment. According to the kinetic analyses, VC and SR dynamics in the triplet manifold occur within 5 ps in DMSO and 50 ps in MeCN. Major conformational changes of the excited states as the origin of the blueshifting is discarded based on the optimized structures. The major geometry change observed is that of the amino group, which is puckered in the $S_2(\pi\pi^*)$ and $T_1(\pi\pi^*)$ states but not in the $S_1(n\pi^*)$ state (Figure S3). The carbon-sulfur bond is also elongated in the excited states but remains planar with the main chromophore.

The population reaching the triplet state of SDMNP decays within 3 ns in DMSO and 60% slower in MeCN (Figure 2c,f). It is notable that ISC back to S_0 occurs so rapidly, which suggests that there is significant SOC between the T_1 and S_0 states. It was examined that the triplet decay is not due to triplet self-quenching by varying the concentration from 75 to 779 μM (Figure S4), supporting the idea that triplet decay is due to an intrinsic process. We note that hundreds of picoseconds ISC back to S_0 has been also observed previously for a selenium-substituted DNA base.[37] Scheme 1a depicts the proposed electronic relaxation mechanism.

Table 1. Extracted lifetimes obtained from global and target analyses for SDMNP and SNR

Lifetime	SDMNP (DMSO)	SDMNP (MeCN)	SNR (DMSO)	SNR (MeCN)
τ_1	580 ± 40 fs	210 ± 40 fs	500 ± 40 fs	540 ± 40 fs
τ_2	5 ± 1 ps	50 ± 2 ps	110 ± 10 ps	41 ± 6 ps
τ_3	440 ± 20 ps	1100 ± 40 ps	∞ (> 3 ns)[a]	∞ (> 3 ns)[a]

[a] A long-lived lifetime (> 3 ns) was required to model the transient signal. Changing its magnitude from 3 to 20 ns does not affect the other two lifetimes.

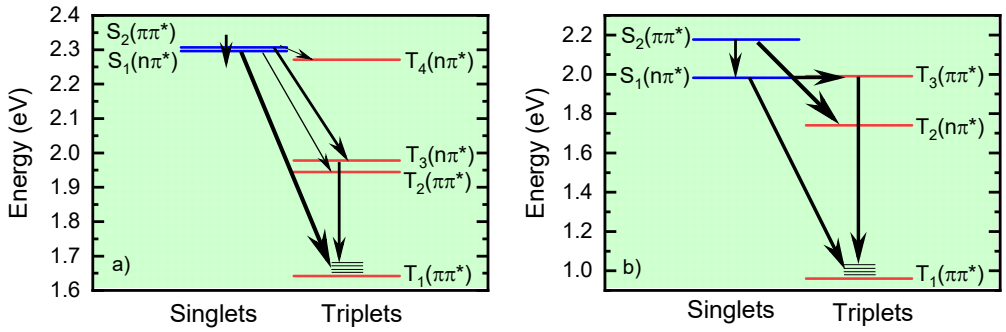

Scheme 1. Proposed deactivation mechanism for SDMNP (a) and SNR (b) in DMSO and MeCN. Thickness of the arrow represents qualitatively the probability of that pathway to occur (the thicker the arrow, the higher the probability).

Figure 4 presents the TAS for SNR following excitation at 674 nm. Positive and negative amplitude bands are observed within the cross-correlation of the pump and probe beams (Figure 4a,b). The negative amplitude bands are assigned to S_0 depopulation, in good agreement with the absorption spectra (Figure 1b). Three positive amplitude absorption bands are also observed with maxima around 405, 450, and 550 nm. Note that a minor absorption band is also observed around 330 nm in both solvents, but it strongly overlaps with the S_0 depopulation signal. The 550 nm band starts to decay during the initial hundreds of femtoseconds in DMSO (Figure 3b), while the other bands stay relatively unchanged. In MeCN, all bands start to decay during the initial hundreds of femtoseconds (Figure 4f). As the 550 nm band continues to decay (Figure 4c, note also the shift to ca. 570 nm), the other two bands start to decay as well (Figure 4f,g). Additionally, the 448 nm band blueshifts (Figure 4c, inset). Figure 4d,g shows that the residual transient signal decays monotonically, but not fully within 3 ns. Representative decay traces, lifetimes extracted from kinetic analyses, and corresponding EADS are reported in Figure 3c,d, Table 1, and Figure S5, respectively.

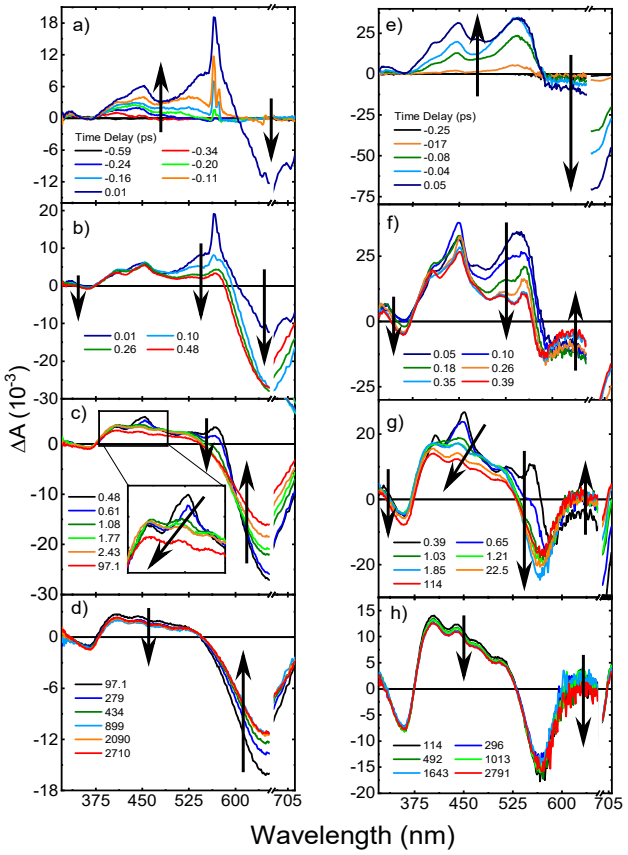

Figure 4. fs-TAS for SNR following 674 nm excitation through a time delay of 3 ns in (a-d) DMSO and (e-g) MeCN solutions. The stimulated Raman emission band of DMSO is observed at 555 nm. This appears within the cross correlation of the pump and probe beams and was used to estimate time zero. In the case of SNR in MeCN, time zero was estimated using the maximum of the 546 nm kinetic trace because the stimulated Raman band from MeCN was not observed. The breaks are covering the scattering of the pump beam reaching the detectors.

The calculations predict that excitation at 674 nm populates the $S_2(\pi\pi^*)$ state directly, which is isoenergetic to the $S_1(n\pi^*)$ and $T_3(\pi\pi)$ states (Table S2). The $S_2(\pi\pi^*)$, $S_1(n\pi^*)$, and $T_1(\pi\pi^*)$ states were optimized and their ESA spectra calculated to assist in the assignment. Attempts to optimize the $T_2(n\pi^*)$ and $T_3(\pi\pi)$ states were unsuccessful. Based on the energy gaps (Table S2), SOCs (Table S5), and calculated ESA spectra (Figure S6), the absorption bands at 330 and 448 nm in Figure 4a,e are assigned to a combination of the $S_1(n\pi^*)$ and $S_2(\pi\pi^*)$ states, while the bands at 405 nm and 550-570 nm are assigned to a high-energy triplet state (i.e., T_2 and/or T_3), the vibrationally excited $T_1(\pi\pi^*)$ state, or a combination of them. This is evident in Figure 3c,d, where the decay trace at 448 nm rapidly decay at early time, followed then a similar decay behavior to the species absorbing 405 nm. Hence, the complex dynamics observed during the first few picoseconds in Figure 4 corresponds to a competition between ultrafast $S_2(\pi\pi^*) \rightarrow S_1(n\pi^*)$ IC and ISC from both singlet states to the triplet manifold (i.e., T_3, T_2, and/or T_1). This combination of

processes occurs within ca. 500 fs (τ_1), largely independent of solvent. As for SDMNP, VC and SR in the triplet manifold occur within τ_2. This is supported by the change of τ_2 with solvent (Table 1). The dynamics in Figure 4d,g correspond to the partial decay of the $T_1(\pi\pi^*)$ state, in top of S_0 repopulation. Scheme 1b depicts the proposed relaxation mechanism.

In this contribution, the deactivation mechanisms of two of the most promising HAF-PSs developed to date[18] were elucidated by combining fs-TAS with ground and excited state calculations, determination of SOCs and ESA of relevant electronic states. Experimental and computational evidence of the primary doorway states leading to ultrafast ISC dynamics were presented. The promising photochemical properties exhibited by these HAF-PSs are due to a straightforward and versatile oxygen-by-sulfur substitution of carbonyl groups. To further get across this point, VEEs and SOCs for dimethylaminonaphtalamide and Nile Red are reported in Tables S6 to S8. The analysis of those calculations provide full support to and further strengthen the notion that thionation is a convenient and general strategy to redshift the absorption spectra, increase the density and the SOCs between the singlet and triplet manifolds of biocompatible organic compounds, ultimately enabling ultrafast ISC, high triplet yields, and effective generation of singlet oxygen.[5, 16, 28, 32] Besides PDT, HAF-PSs such as SDMNP and SNR are anticipated to find wide-ranging applications in photocatalysis, photovoltaics, organic LEDs, and photon up-conversion.

ASSOCIATED CONTENT

Supporting Information

The Supporting Information is available free of charge at https://pubs.acs.org/doi/

Experimental and computational methods; tables and figures with vertical excitation energies and oscillator strengths, spin-orbit coupling constants, optimized excited state geometries and Cartesian coordinates, and discussion of supporting results.

Notes

The authors declare no competing financial interest.

Acknowledgement

L.A.O-.R., S.J.H., and C.E.C.-H. acknowledge the National Science Foundation (Grant No. CHE-1800052). L.A.O-.R. also acknowledge the NSF-AGEP program for support. This work made use of the High Performance Computing Resource in the Core Facility for Advanced Research Computing at CWRU. A.L., L.W., and H.X. acknowledge the Cancer Prevention Research Institute of Texas (CPRIT RR170014), NIH (R35-GM133706), the Robert A. Welch Foundation (C-1970), the John S. Dunn Foundation Collaborative Research Award, and the Hamill Innovation Award. H.X. is a Cancer Prevention & Research Institute of Texas (CPRIT) Scholar in Cancer Research.

References

1. Dougherty, T. J.; Gomer, C. J.; Henderson, B. W.; Jori, G.; Kessel, D.; Korbelik, M.; Moan, J.; Peng, Q., Photodynamics Therapy. *J. Natl. Cancer Inst.* **1998,** *90*, 889-905.

2. Macdonald, I. J.; Dougherty, T. J., Basic principles of photodynamic therapy. *J. Porphyr. Phthalocyanines* **2001,** *5*, 105-129.
3. Castano, A. P.; Demidova, T. N.; Hamblin, M. R., Mechanisms in photodynamic therapy: part one—photosensitizers, photochemistry and cellular localization. *Photodiagnosis Photodyn. Ther.* **2004,** *1* (4), 279-293.
4. Castano, A. P.; Mroz, P.; Hamblin, M. R., Photodynamic therapy and anti-tumor immunity. *Nat. Rev. Cancer* **2006,** *6* (7), 535-545.
5. Ortiz-Rodríguez, L. A.; Crespo-Hernández, C. E., Thionated organic compounds as emerging heavy-atom-free photodynamic therapy agents. *Chem. Sic.* **2020,** *11*, 11113-11123.
6. Dolmans, D. E. J. G. J.; Fukumura, D.; Jain, R. K., Photodynamic therapy for cancer. *Nat. Rev. Cancer* **2003,** *3*, 380-387.
7. Brown, S. B.; Brown, E. A.; Walker, I., The present and future role of photodynamic therapy in cancer. *Lancet Oncol.* **2004,** *5* (8), 497-508.
8. Fan, W.; Huang, P.; Chen, X., Overcoming the Achilles' heel of photodynamic therapy. *Chem. Soc. Rev.* **2016,** *45*, 6488-6519.
9. Abrahamse, H.; Hamblin, Michael R., New photosensitizers for photodynamic therapy. *Biochem. J.* **2016,** *473* (4), 347-364.
10. Agostinis, P.; Berg, K.; Cengel, K. A.; Foster, T. H.; Girotti, A. W.; Gollnick, S. O.; Hahn, S. M.; Hamblin, M. R.; Juzeniene, A.; Kessel, D.; Korbelik, M.; Moan, J.; Mroz, P.; Nowis, D.; Piette, J.; Wilson, B. C.; Golab, J., Photodynamics therapy of cancer: an update. *CA: Cancer J. Clin.* **2011,** *61*, 250-281.
11. Allison, R. R.; Sibata, C. H., Oncologic photodynamic therapy photosensitizers: a clinical review. *Photodiagnosis Photodyn. Ther.* **2010,** *7* (2), 61-75.
12. Bruijnincx, P. C. A.; Sadler, P. J., Controlling platinum, ruthenium, and osmium reactivity for anticancer drug design. *Adv. Inorg. Chem.* **2009,** *61*, 1-62.
13. Smith, N. A.; Sadler, P. J., Photoactivatable metal complexes: from theory to applications in biotechnology and medicine. *Phil. Trans. R. Soc. A* **2013,** *371*, 20120519.
14. Monro, S.; Colón, K. L.; Yin, H.; Roque III, J.; Konda, P.; Gujar, S.; Thummel, R. P.; Lilge, L.; Cameron, C. G.; McFarland, S. A., Transition metal complexes and photodynamic therapy from a tumor-centered approach: challenges, opportunities, and highlights from the development of TLD1433. *Chem. Rev.* **2019,** *119* (2), 797-828.
15. Pollum, M.; Jockusch, S.; Crespo-Hernández, C. E., 2, 4-Dithiothymine as a potent UVA chemotherapeutic agent. *J. Am. Chem. Soc.* **2014,** *136* (52), 17930-17933.
16. Ashwood, B.; Pollum, M.; Crespo-Hernández, C. E., Photochemical and photodynamical properties of sulfur-substituted nucleic acid bases. *Photochem. Photobiol.* **2019,** *95* (1), 33-58.
17. Nguyen, V.-N.; Qi, S.; Kim, S.; Kwon, N.; Kim, G.; Yim, Y.; Park, S.; Yoon, J., An emerging molecular design approach to heavy-atom-free photosensitizers for enhanced photodynamic therapy under hypoxia. *J. Am. Chem. Soc.* **2019,** *141*, 16243-16248.
18. Tang, J.; Wang, L.; Loredo, A.; Cole, C.; Xiao, H., Single-atom replacement as a general approach towards visible-light/near-infrared heavy-atom-free photosensitizers for photodynamic therapy. *Chem. Sci.* **2020,** *11*, 6701-6708.
19. Pollum, M.; Guan, L.; Ahsanuddin, S.; Baron, E.; Lam, M.; Crespo-Hernández, C., Photoactivation of sulfur-modified DNA and RNA analogs induces cytotoxicity in epidermoid carcinoma cells. *J. Invest. Dermatol.* **2016,** *136*, S105.

20. Pollum, M.; Minh, L.; Jockusch, S.; Crespo-Hernández, C. E., Dithionated nucleobases as effective photodynamic agent against human epidermoid carcinoma cells. *ChemMedChem* **2018,** *13*, 1044-1050.
21. Tang, J.; Robichaux, M. A.; Wu, K.-L.; Pei, J.; Nguyen, V.-N.; Zhou, Y.; Wensel, T. G.; Xiao, H., Single-atom fluorescence switch: a general approach toward visible-light-activated dyes for biological imaging. *J. Am. Chem. Soc.* **2019,** *141*, 14699-14706.
22. Lower, S. K.; El-Sayed, M. A., The triplet state and molecular electronic processes in organic molecules. *Chem. Rev.* **1966,** *66*, 199-241.
23. El-Sayed, M. A., Triplet state. Its radiative and nonradiative properties. *Acc. Chem. Res.* **1968,** *1*, 8-16.
24. Reichardt, C.; Crespo-Hernández, C. E., Room-temperature phosphorescence of the DNA monomer analogue 4-thiothymidine in aqueous solutions after UVA excitation. *J. Phys. Chem. Lett.* **2010,** *1* (15), 2239-2243.
25. Reichardt, C.; Guo, C.; Crespo-Hernández, C. E., Excited-state dynamics in 6-thioguanosine from the femtosecond to microsecond time scale. *J. Phys. Chem. B.* **2011,** *115* (12), 3263-3270.
26. Pollum, M.; Martínez-Fernández, L.; Crespo-Hernández, C. E., Photochemistry of nucleic acid bases and their thio-and aza-analogues in solution. In *Photoinduced Phenomena in Nucleic Acids I*, Barbatti, M. B., A. C.; U. Susanne, Ed. Springer, Cham: Switzerland, 2015; Vol. 355, pp 245-327.
27. Pollum, M.; Jockusch, S.; Crespo-Hernández, C. E., Increase in the photoreactivity of uracil derivatives by doubling thionation. *Phys. Chem. Chem. Phys.* **2015,** *17* (41), 27851-27861.
28. Mai, S.; Pollum, M.; Martínez-Fernández, L.; Dunn, N.; Marquetand, P.; Corral, I.; Crespo-Hernández, C. E.; González, L., The origin of efficient triplet state population in sulfur-substituted nucleobases. *Nature Commun.* **2016,** *7*, 13077.
29. Martínez-Fernández, L.; Granucci, G.; Pollum, M.; Crespo-Hernández, C.; Persico, M.; Corral, I., Decoding the molecular basis for the population mechanism of the triplet phototoxic precursors in UVA light-activated pyrimidine anticancer drugs. *Chem. Eur. J.* **2017,** *23*, 2619-2627.
30. Borrego-Varillas, R.; Teles-Ferreira, D. C.; Nenov, A.; Conti, I.; Ganzer, L.; Manzoni, C.; Garavelli, M.; de Paula, A. M.; Cerullo, G., Observation of the sub-100 femtosecond population of a dark state in a thiobase mediating intersystem crossing. *J. Am. Chem. Soc.* **2018,** *140*, 16087-16093.
31. Teles-Ferreira, D.; Conti, I.; Borrego-Varillas, R.; Nenov, A.; van Stokkum, I. H. M.; Ganzer, L.; Manzoni, C.; de Paula, A. M.; Cerullo, G.; Garavelli, M., A unified experimental/theoretical description of the ultrafast photophysics of single and double thionated uracils. *Chem. Eur. J.* **2019**, DOI: 10.1002/chem.201904541.
32. Ortiz-Rodríguez, L. A.; Reichardt, C.; Hoehn, S. J.; Jockusch, S.; Crespo-Hernández, C. E., Detection of the thietane precursor in the UVA formation of the DNA 6-4 photoadduct. *Nat. Commun.* **2020,** *11*, 3599.
33. Ashwood, B.; Ortiz-Rodríguez, L. A.; Crespo-Hernández, C. E., Photochemical relaxation pathways of S^6-methylthioinosine and O^6-methylguanosine in solution. *Faraday Discuss.* **2018,** *207*, 351-374.
34. Tilley, A. J.; Pensack, R. D.; Lee, T. S.; Djukic, B.; Scholes, G. D.; Seferos, D. S., Ultrafast triplet formation in thionated perylene diimides. *J. Phys. Chem. C* **2014,** *118*, 9996-10004.

35. Pollum, M.; Ashwood, B.; Jockusch, S.; Lam, M.; Crespo-Hernández, C. E., Unintended consequences of expanding the genetic alphabet. *J. Am. Chem. Soc.* **2016,** *138* (36), 11457-11460.
36. Ashwood, B.; Jockusch, S.; Crespo-Hernández, C. E., Photoreactivity of dTPT3: An unnatural nucleoside for developing semi-synthetic organisms. *J. Phys. Chem. Lett.* **2017,** *8*, 2387-2392.
37. Farrell, K. M.; Brister, M. M.; Pittelkow, M.; Sølling, T. I.; Crespo-Hernández, C. E., Heavy-atom-substituted nucleobases in photodynamic applications: substitution of sulfur with selenium in 6-thioguanine induces a remarkable increase in the rate of triplet decay in 6-selenoguanine. *J. Am. Chem. Soc.* **2018,** *140*, 11214-11218.